



**Evaluation of CH<sub>4</sub> Oxidation Activity of High-Valent Iron-Oxo Species of A  $\mu$ -Nitrido-Bridged Heterodimer of Iron Porphycene and Iron Phthalocyanine**

Journal:	<i>Catalysis Science &amp; Technology</i>
Manuscript ID	CY-ART-11-2022-001980.R1
Article Type:	Paper
Date Submitted by the Author:	16-Jan-2023
Complete List of Authors:	Yamada, Yasuyuki; Nagoya University - Higashimaya Campus Miwa, Yusuke; Nagoya University - Higashimaya Campus, Department of Chemistry, Graduate School of Science Toyoda, Yuka; Nagoya Daigaku, Research Center for Materials Science Phung, Quan Manh; Nagoya University, Chemistry; Nagoya University, Institute of Transformative Bio-Molecules (WPI-ITbM) Oyama, Kin-Ichi; Nagoya University, Research Institute for Materials Science Tanaka, Kentaro; Nagoya University, Department of Chemistry, Graduate School of Science

## PAPER

## Evaluation of CH<sub>4</sub> Oxidation Activity of High-Valent Iron-Oxo Species of A $\mu$ -Nitrido-Bridged Heterodimer of Iron Porphycene and Iron Phthalocyanine

Received 00th January 20xx,  
Accepted 00th January 20xx

DOI: 10.1039/x0xx00000x

Yasuyuki Yamada,<sup>\*a,b</sup> Yusuke Miwa,<sup>a</sup> Yuka Toyoda,<sup>b</sup> Quan Manh Phung,<sup>a,c</sup> Kin-ichi Oyama<sup>b</sup> and Kentaro Tanaka<sup>\*a</sup>

A  $\mu$ -nitrido-bridged dimer of iron phthalocyanine is one of the most potent molecule-based CH<sub>4</sub> oxidation catalysts reported to date. The reactive intermediate is a high-valent iron-oxo species generated through reaction with H<sub>2</sub>O<sub>2</sub> in an acidic aqueous solution. However, there are few reports on the synthesis and catalytic CH<sub>4</sub> oxidation activity of a  $\mu$ -nitrido-bridged heterodimer of two different iron porphyrinoids, despite that there are a variety of iron porphyrinoids with coordination and electronic structures different from those of iron phthalocyanines or iron porphyrins. Herein, we report the synthesis of a novel  $\mu$ -nitrido-bridged heterodimer of an iron phthalocyanine and iron porphycene and examine its CH<sub>4</sub> oxidation activity. Porphycenes are an important class of porphyrinoids with a smaller coordination sphere than phthalocyanines or porphyrins. Single crystal structural analyses revealed that the heterodimer possessed a Fe–N=Fe core structure similar to that of the phthalocyanine homodimer. The heterodimer showed catalytic CH<sub>4</sub> oxidation activity in an acidic aqueous solution in the presence of H<sub>2</sub>O<sub>2</sub> at 60 °C through the high-valent iron-oxo species as in the case with the phthalocyanine homodimer. This was in clear contrast to the result that the high-valent iron-oxo species of a  $\mu$ -nitrido-bridged iron porphycene dimer was so unstable that it decomposed quickly in the same reaction condition.

### Introduction

Several decades have passed since some methane monooxygenases (MMOs) were found to utilize high-valent iron-oxo species as reaction intermediates for the catalytic conversion of CH<sub>4</sub> into CH<sub>3</sub>OH under ambient reaction conditions.<sup>1–4</sup> CH<sub>4</sub> has long been expected to be the next-generation carbon resource because it is abundant in nature as natural gas or methane hydrate.<sup>5,6</sup> However, CH<sub>4</sub> is a stable organic compound with a particularly high C–H bond dissociation energy of *ca.* 105 kcal mol<sup>-1</sup>.<sup>7</sup> Therefore, the development of an efficient catalyst is indispensable for low-cost and efficient conversion of CH<sub>4</sub> into industrially useful chemical raw materials such as CH<sub>3</sub>OH.<sup>6,8</sup> Therefore, it is quite understandable that the fact that some MMOs achieve efficient catalytic conversion of CH<sub>4</sub> into CH<sub>3</sub>OH at ambient temperature by utilizing high-valent iron-oxo species has stimulated the interest of chemists to fabricate a large variety of biomimetic iron-oxo-based molecular catalysts.<sup>9–17</sup> The detailed reaction mechanisms of natural MMOs have been

clarified as a result of utilizing these biomimetic catalysts. The CH<sub>4</sub> oxidation reaction by high-valent iron-oxo species is facilitated by the proton-coupled electron transfer (PCET) pathway, enabling low-temperature and efficient CH<sub>4</sub> oxidation.<sup>18,19</sup>

However, from the viewpoint of catalytic activity, a very limited number of artificial molecular iron-oxo-based biomimetic catalysts exist that activate the C–H bonding of CH<sub>4</sub> at temperatures lower than 100 °C because of the high stability of CH<sub>4</sub>.<sup>3,18,20</sup> A. B. Sorokin et al. found that a  $\mu$ -nitrido-bridged iron phthalocyanine (Pc) dimer (**1** or **1**<sup>+</sup>) react with H<sub>2</sub>O<sub>2</sub> in an acidic aqueous solution to afford a high-valent iron-oxo species **1**<sub>oxo</sub>, which shows a particularly high CH<sub>4</sub> oxidation activity among various molecular CH<sub>4</sub> oxidation catalysts at a lower temperature than 100 °C (Figure 1a).<sup>20–22</sup> Similarly,  $\mu$ -nitrido-bridged iron porphyrin dimer **2** was reported to indicate CH<sub>4</sub> oxidation activity comparable to that of  $\mu$ -nitrido-bridged iron phthalocyanine dimer (Figure 1b).<sup>23</sup> According to some theoretical estimates, the core  $\mu$ -nitrido-bridged dinuclear iron structure (Fe–N=Fe) is believed to be crucial in the reaction of these high CH<sub>4</sub> oxidation activities.<sup>24–27</sup>

Inspired by these previous works, we recently synthesized  $\mu$ -nitrido-bridged dinuclear iron porphycene (Ppc) dimer **3**<sup>+</sup>, a structural analog of **1**<sup>+</sup>, and investigated its CH<sub>4</sub> oxidation activity (Figure 1c).<sup>28</sup> Porphycene is an important class of porphyrinoids and has a rectangular-shaped narrower cavity than phthalocyanine, which renders the coordination structures and reactivities of the metal complexes different from those of phthalocyanine.<sup>29,30</sup>

<sup>a</sup> Department of Chemistry, Graduate School of Science, Nagoya University, Furo-cho, Chikusa-ku, Nagoya 464-8602, Japan.

<sup>b</sup> Research Center for Materials Science, Nagoya University, Furo-cho, Chikusa-ku, Nagoya 464-8602, Japan.

<sup>c</sup> Institute of Transformative Bio-Molecules (ITBM), Nagoya University, Furo-cho, Chikusa-ku, Nagoya 464-8602, Japan.

†E-mail: [yv@chem.nagoya-u.ac.jp](mailto:yv@chem.nagoya-u.ac.jp), [kentaro@chem.nagoya-u.ac.jp](mailto:kentaro@chem.nagoya-u.ac.jp)

Electronic Supplementary Information (ESI) available: [details of any supplementary information available should be included here]. See DOI: 10.1039/x0xx00000x

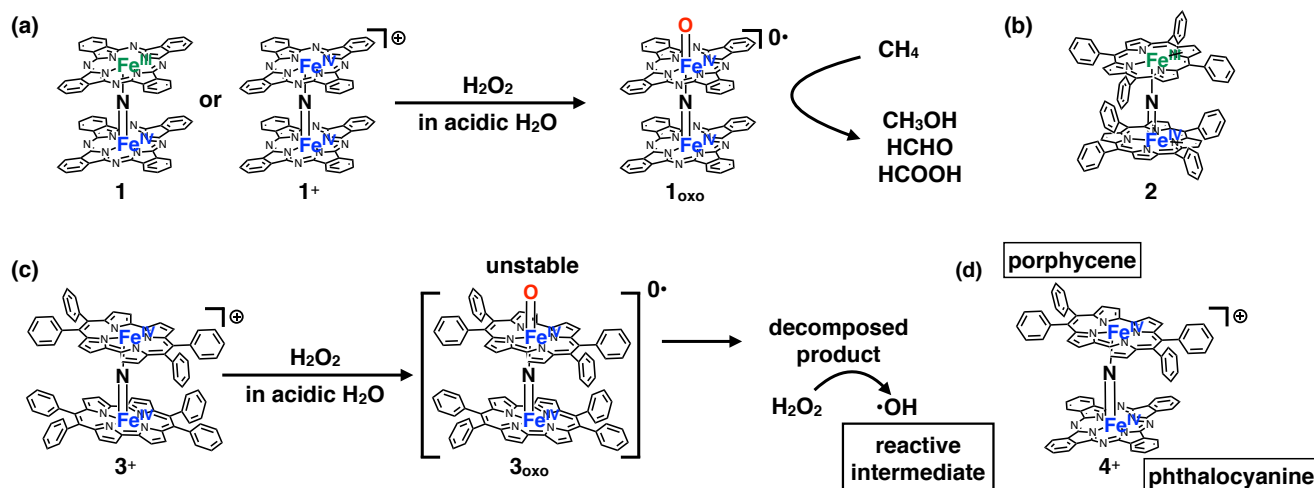


**Figure 1** (a) Formation of high-valent iron oxo species  $1_{\text{oxo}}$  having a potent  $\text{CH}_4$  oxidation ability, from  $1$  or  $1^+$  through the reaction with  $\text{H}_2\text{O}_2$ . (b) A  $\mu$ -nitrido-bridged iron porphyrin dimer ( $2$ ) showing a potent  $\text{CH}_4$  oxidation ability. (c) Structure of a monocationic  $\mu$ -nitrido-bridged iron porphycene dimer ( $3^+$ ) and its proposed  $\text{CH}_4$  oxidation mechanism. (d) A monocationic  $\mu$ -nitrido-bridged heterodimer of an iron porphycene and an iron phthalocyanine ( $4^+$ ) synthesized in this work.

Although  $3^+$  has a  $\mu$ -nitrido-bridged dinuclear iron core ( $\text{Fe}-\text{N}=\text{Fe}$ ) similar to that of  $1^+$ , it was found that  $3^+$  showed less  $\text{CH}_4$  oxidation activity, and the reaction proceeded through a different mechanism (Fenton-type reaction; the reaction intermediate is  $\bullet\text{OH}$ ). This is presumably because the high-valent iron-oxo species  $3_{\text{oxo}}$  is less stable than  $1_{\text{oxo}}$  and decomposes during the  $\text{CH}_4$  oxidation reaction. The decomposed product could act as a catalyst for  $\bullet\text{OH}$  production. These results indicate that the difference in the structure of the porphyrinoid moiety strongly affects the reactivity of the high-valent iron-oxo species.

In this study, we report the synthesis of a  $\mu$ -nitrido-bridged heterodimer of an iron phthalocyanine and iron porphycene  $4^+$  (Figure 1d) and its  $\text{CH}_4$  oxidation activity. Thus far, there have been very few reports investigating the  $\text{CH}_4$  oxidation activity of  $\mu$ -nitrido-bridged heterodimers of iron porphyrinoids. We previously confirmed that a supramolecular  $\mu$ -nitrido-bridged heterodimer of an iron porphyrin and iron phthalocyanine provided sufficiently stable high-valent iron-oxo species for catalytic  $\text{CH}_4$  or  $\text{CH}_3\text{CH}_3$  oxidation reactions.<sup>31,32</sup> It has also been reported that  $\text{H}_2\text{O}_2$  preferentially reacts with the electron-rich iron phthalocyanine moiety of the  $\mu$ -nitrido-bridged heterodimer of an electron-rich iron phthalocyanine and an electron-deficient iron phthalocyanine to afford a high-valent iron-oxo species, although the reactivity of the heterodimer has not been reported.<sup>33</sup> Therefore, the fact that a  $\mu$ -nitrido-bridged iron phthalocyanine dimer  $1$  or  $1^+$  indicated potent  $\text{CH}_4$  oxidation activity through the reaction of high-valent iron-oxo species, whereas a  $\mu$ -nitrido-bridged dinuclear iron porphycene dimer  $3^+$  showed a different  $\text{CH}_4$  oxidation mechanism, prompted us to clarify the relationship between the structure and reactivity of  $4^+$ .

## Results and Discussion

### Synthesis and Spectroscopic Characterization of $4^+$ .

A mixture of iron porphycene **5** and iron phthalocyanine **6** was heated in 1-chloronaphthalene in the presence of excess  $\text{NaN}_3$  at  $280^\circ\text{C}$ , followed by oxidation with iodine to yield a monocationic  $\mu$ -nitrido-bridged heterodimer of an iron phthalocyanine and iron

porphycene  $4^+\cdot\text{I}_3^-$  (Figure 2a). When an equimolar mixture of iron porphycene **5** and iron phthalocyanine **6** was heated, the isolated yield of the desired compound,  $4^+\cdot\text{I}_3^-$ , was relatively low (ca. 10%). This is because a significant amount of the  $\mu$ -nitrido-bridged iron phthalocyanine dimer was obtained (ca. 40%), suggesting that the formation of the  $\mu$ -nitrido-bridged iron phthalocyanine dimer was faster than the formation of the desired heterodimer under these reaction conditions. Therefore, heating a 2:1 mixture of iron porphycene **5** and iron phthalocyanine **6** with  $\text{NaN}_3$  improved the isolated yield of  $4^+\cdot\text{I}_3^-$  to 71%. Elemental analysis suggested that the counter anion of the monocationic heterodimer was triiodide, which was further confirmed using single-crystal X-ray structural analysis.

$^1\text{H-NMR}$  and MALDI-TOF MS analyses were performed to characterize  $4^+\cdot\text{I}_3^-$ . In the MALDI-TOF MS spectrum shown in Figure S1 in the Supporting Information, a signal corresponding to  $4^+$  was observed at  $m/z = 1250.26$ , which corresponds to the theoretical isotope distribution pattern of  $4^+$ . As shown in Figure 2b, all the  $^1\text{H-NMR}$  peaks of  $4^+\cdot\text{I}_3^-$  were observed as sharp signals in the range of 6–10 ppm. A neutral  $\mu$ -nitrido-bridged FeTPP dimer containing Fe(III) and Fe(IV) was reported to indicate a significant broadening of the  $^1\text{H-NMR}$  signals, whereas its monocationic species containing two Fe(IV) centers showed sharp  $^1\text{H-NMR}$  signals because the two Fe(IV) centers interacted with each other in an antiferromagnetic manner.<sup>34–36</sup> Therefore, it is considered that  $4^+\cdot\text{I}_3^-$  includes two Fe(IV) ions interacting with each other in an antiferromagnetic manner. Moreover, considering that two sets of signals corresponding to those of the *o*- and *m*-protons of the peripheral phenyl groups were observed, the rotation of the peripheral phenyl groups of the porphycene ring was restricted owing to steric repulsion between the phenyl groups and porphycene ring, as in the case of the previously reported  $\mu$ -nitrido-bridged dinuclear iron porphycene dimer  $3^+\cdot\text{PF}_6^-$ . However, the rotation of the porphycene ring along the  $\text{Fe}-\text{N}=\text{Fe}$  axis was sufficiently fast compared to the NMR timescale because the porphycene ring was observed as a  $\text{C}_2$  symmetrical structure.

A comparison of the UV-Vis spectra of  $4^+\text{-PF}_6^-$  with those of  $\mu$ -nitrido-bridged iron phthalocyanine dimer  $1^+\text{-I}^-$  and  $\mu$ -nitrido-bridged iron porphycene dimer  $3^+\text{-PF}_6^-$  is shown in Figure 3. The bands at 357 and 399 nm were assignable to phthalocyanine and porphycene, respectively, both of which showed significant shifts compared to those of the homoleptic dimers  $1^+\text{-I}^-$  and  $3^+\text{-PF}_6^-$ .<sup>28,37</sup> The Q-band of the phthalocyanine unit of  $4^+\text{-PF}_6^-$  at 634 nm showed an apparent hypochromic shift compared to that of the phthalocyanine dimer  $1^+\text{-I}^-$ , whereas the Q-band of the phthalocyanine units of  $4^+\text{-PF}_6^-$  at 705 nm appeared at a higher wavelength than that of  $1^+\text{-I}^-$ . These results implied an apparent electronic interaction between the two porphyrinoids in  $4^+\text{-PF}_6^-$ .

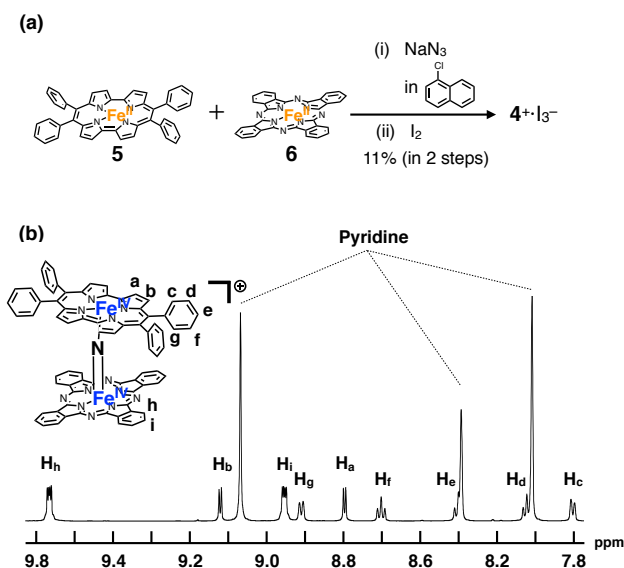


**Figure 2** (a) Synthesis of a monocationic heterodimer  $4^+\text{-I}_3^-$ . (b)  $^1\text{H-NMR}$  spectrum of  $4^+\text{-I}_3^-$  in  $\text{pyridine-d}_5$ .

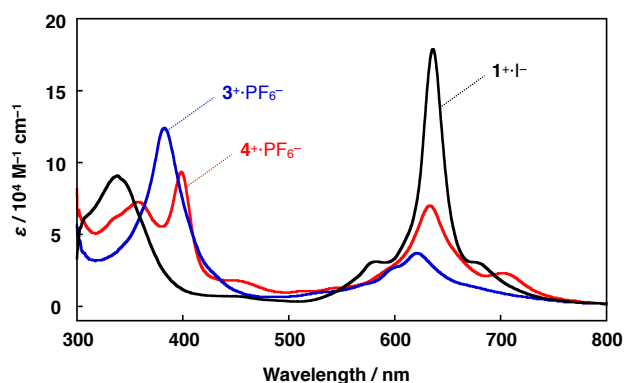


**Figure 3** (a) Comparison of UV-Vis spectra of a heterodimer  $4^+\text{-PF}_6^-$  and two homodimers  $1^+\text{-I}^-$  and  $3^+\text{-PF}_6^-$  in pyridine at 20 °C.

#### Single Crystal X-Ray Structural Analysis.

Crystal structural analysis of  $4^+\text{-I}_3^-$  demonstrated that  $4^+\text{-I}_3^-$  crystallized in the monoclinic space group  $P21/c$  from a solution of 1:1 (v/v) mixture of pyridine and  $\text{CHCl}_3$ . The molecular structures of  $4^+\text{-I}_3^-$  are shown in Figure 4a and 4b.

The distance between the  $\mu$ -nitrogen and Fe(IV) ions in porphycene (1.62(9) Å) is almost identical to that of the  $\mu$ -nitrogen and Fe(IV) ions in phthalocyanine (1.66(4) Å), suggesting that the Fe– $\mu$ -N–Fe core has a  $\pi$ -conjugated structure. The mean bond distances between the four porphycene nitrogens and the coordinated Fe(IV) ion (1.93 Å) are almost identical to those between the four phthalocyanine nitrogens and the coordinated Fe(IV) ion (1.94 Å). The average bond angles of the  $\mu$ -nitrogen–Fe–nitrogens (porphyrinoid) in  $4^+\text{-I}_3^-$  were 93.45(8)° for iron phthalocyanine and 93.13(3)° for iron porphycene, both of which were slightly larger than 90°. The core-coordinating N4 planes of the two porphyrinoid rings are located in an almost parallel configuration. The phthalocyanine ring was slightly distorted from the planar structure, presumably because of steric repulsion between the phthalocyanine ring and peripheral phenyl group of the porphycene ring. As suggested by  $^1\text{H-NMR}$  spectroscopy, the rotation of the peripheral phenyl groups of the porphycene ring appeared to be significantly suppressed by steric repulsion between the phenyl groups and porphycene rings.

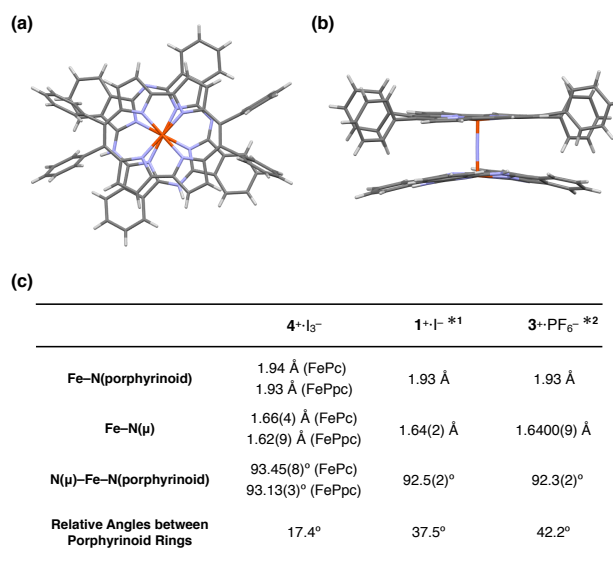


**Figure 4** (a) Side and (b) top views of the single crystal X-ray structure of  $4^+\text{-I}_3^-$ .  $\text{I}_3^-$ , coordinating pyridines, and crystalline solvents were omitted for clarity. (c) Comparison of some mean bond lengths and angles of  $4^+\text{-I}_3^-$ ,  $1^+\text{-I}^-$ , and  $3^+\text{-PF}_6^-$ . \*1: Ref. 28, \*2: Ref. 38.

A comparison of the single-crystal structure of  $4^+\text{-I}_3^-$  with those of  $1^+\text{-I}^-$  and  $3^+\text{-PF}_6^-$  is summarized in a table shown in Figure 4c.<sup>28,38</sup> Although slight differences were observed in the distance between nitrogen and Fe(IV) and the average bond angles of the  $\mu$ -nitrogen–Fe–nitrogen (porphyrinoid), these differences are presumably derived from the heteroleptic structure of  $4^+\text{-I}_3^-$ . Overall, it could be concluded that  $4^+\text{-I}_3^-$  has a similar Fe–N–Fe core structure to those of  $1^+\text{-I}^-$  and  $3^+\text{-PF}_6^-$ . The relative angle between the phthalocyanine ring and the long axis of the porphycene ring was calculated to be 17.4°, which was much smaller than the relative angles between the two porphyrinoid rings in  $1^+\text{-I}^-$  (37.5°) and  $3^+\text{-PF}_6^-$  (42.2°). We attributed this difference in the relative angle between the two



porphyrinoids to the difference in the packing structure, because both rings in  $4^+ \cdot I_3^-$  are rotatable along the Fe–N=Fe axis.

### Cyclic Voltammetric Analysis.

Cyclic voltammograms of  $4^+ \cdot PF_6^-$  were recorded in a pyridine solution (200  $\mu$ M) containing 100 mM  $nBu_4N^+ \cdot PF_6^-$ . A comparison of the voltammograms of the  $\mu$ -nitrido-bridged iron phthalocyanine dimer  $1^+ \cdot I^-$  and  $\mu$ -nitrido-bridged iron porphycene dimer  $3^+ \cdot PF_6^-$  is shown in Figure 5b, 5c.  $4^+ \cdot PF_6^-$  showed four quasi-reversible redox waves at  $-0.75$ ,  $-1.37$ ,  $-1.69$  and  $-1.92$  V vs. Fc/Fc $^+$  and one irreversible oxidation wave at 0.50 V.

In the case of a voltammogram of a  $\mu$ -nitrido-bridged iron phthalocyanine dimer  $1^+ \cdot I^-$  (shown in Figure 5b), Ercolani et al. carefully investigated the redox processes to conclude that the four redox waves at  $-0.58$ ,  $-1.52$ ,  $-1.74$  and  $-2.00$  V should be assignable to the redox in the iron cores of  $1^+ \cdot I^-$ .<sup>39</sup> For the voltammogram of a  $\mu$ -nitrido-bridged iron porphycene dimer  $3^+ \cdot PF_6^-$  shown in Figure 5c, we assigned the 1st ( $-0.90$  V vs. Fc $^+$ /Fc), 2nd ( $-1.32$  V), 3rd ( $-1.49$  V), and 4th ( $-1.78$  V) reduction waves of the porphycene dimer to those of Fe(IV)Fe(IV)/Fe(III)Fe(IV), Fe(III)Fe(IV)/Fe(III)Fe(III), Fe(III)Fe(III)/Fe(II)Fe(III), and Fe(II)Fe(III)/Fe(II)Fe(II), respectively. This is based on the fact that Gross *et al.* investigated the detailed redox properties of a 2,7,12,17-tetra-*n*-propylporphycene iron (III) chloride (ClFeTprPpc), a monomeric porphycene, by electrochemical and spectroelectrochemical measurements to report that the reduction of the iron center (Fe(III)/Fe(II)) occurred at more positive potential than that of the porphycene center (TprPpc/TprPpc $^{\cdot-}$ ).<sup>40</sup> Similarly, it is assumed that at least the four reduction waves of  $4^+ \cdot PF_6^-$  at  $-0.75$ ,  $-1.37$ ,  $-1.69$ , and  $-1.92$  V could be assignable to those of the iron center of  $4^+ \cdot PF_6^-$ . Thus, it was demonstrated that  $4^+ \cdot PF_6^-$  has a completely different electronic structure from those of  $1^+ \cdot I^-$  and  $3^+ \cdot PF_6^-$  owing to the different types of porphyrinoid rings.<sup>38</sup>

As for the oxidation of  $4^+ \cdot PF_6^-$ , theoretical calculations suggested that the phthalocyanine ring is more easily oxidized than the porphycene ring (*vide infra*, see "DFT calculations" section). In

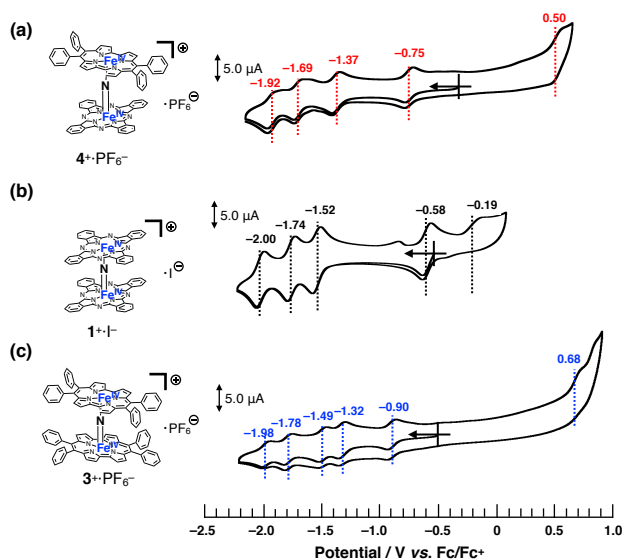


**Figure 5** Comparison of cyclic voltammograms of (a)  $4^+ \cdot PF_6^-$ , (b)  $1^+ \cdot I^-$ , and (c)  $3^+ \cdot PF_6^-$  in a pyridine solution containing 100 mM of  $nBu_4N^+ \cdot PF_6^-$  at room temperature. [Substrate] = 200  $\mu$ M, [Scan rate] = 100 mV/s.

addition, the  $\mu$ -nitrido-bridged iron phthalocyanine dimer  $1^+ \cdot I^-$  showed a lower oxidation potential at  $-0.19$  V than that of a  $\mu$ -nitrido-bridged iron porphycene dimer  $3^+ \cdot PF_6^-$  at 0.68 V, both of which are assignable to the oxidations of porphyrinoid cores. Therefore, the oxidation wave at 0.50 V is assignable to that of the phthalocyanine ring. Overall,  $4^+ \cdot PF_6^-$  showed a first reduction wave higher than  $1^+ \cdot I^-$  and lower than  $3^+ \cdot PF_6^-$ , whereas the first oxidation wave of  $4^+ \cdot PF_6^-$  was observed at potentials higher than  $1^+ \cdot I^-$  and lower than  $3^+ \cdot PF_6^-$ .

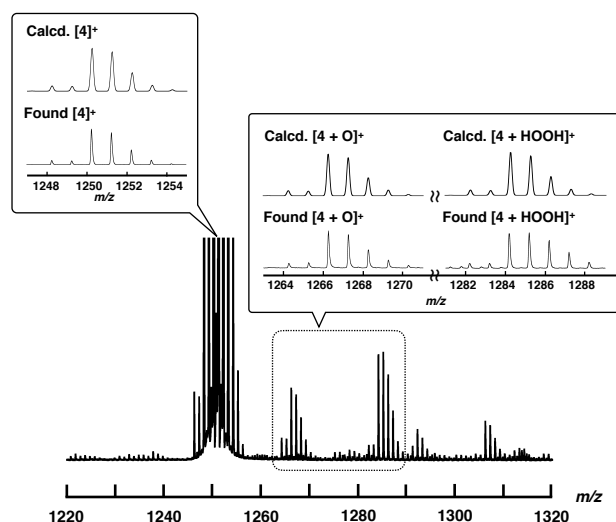


**Figure 6** ESI-TOF MS spectrum of  $4^+ \cdot I_3^-$  in an aqueous  $CH_3CN$  solution containing excess amount of  $H_2O_2$  at room temperature (the detail of the experimental procedure is shown in the Experimental Section). Insets: Comparison of calculated (top) and experimental (bottom) isotopic distribution patterns of molecular peaks assignable to  $[4]^+$ ,  $[4 + O]^+$ , and  $[4 + HOOH]^+$ .

### ESI-TOF MS Analysis of High-Valent Iron-Oxo Species.

To confirm the generation of high-valent iron-oxo species, the reactive intermediate for the oxidation reaction, by treating  $4^+ \cdot I_3^-$  with  $H_2O_2$  in an aqueous solution, ESI-TOF MS measurement of an acetonitrile solution of  $4^+ \cdot I_3^-$  in the presence of  $H_2O_2$  was performed.

As shown in Figure 6, the signals assignable to those of the high-valent iron-oxo species ( $[4 + O]^+$ ) were observed at approximately  $m/z = 1266$  after the addition of aqueous  $H_2O_2$  at room temperature, with its isotopic distribution pattern corresponding to that of the calculated pattern. The signals observed at approximately 1284 correspond to those of the hydroperoxo species ( $[4 + HOOH]^+$ ). We also confirmed that treatment of  $4^+ \cdot I_3^-$  with  $H_2^{18}O_2$  resulted in the generation of the peaks assignable to  $[4 + ^{18}O]$  as shown in the Supporting Information. These results demonstrate that high-valent iron-oxo species were generated after the threat of  $4^+$  with  $H_2O_2$  via the corresponding hydroperoxo species, as in the case with the other  $\mu$ -nitrido-bridged iron phthalocyanine dimers. Sorokin et al. reported that treatment of heteroleptic  $\mu$ -nitrido-bridged dimer of iron phthalocyanine and iron porphyrine with *m*-chloroperbenzoic acid (*m*CPBA) resulted in the attachment of oxo moiety either on the iron phthalocyanine and iron porphyrine. In this case, they concluded that the attachment of oxo moiety occurred with slight preference for the

iron phthalocyanine unit based on the results of cryospray collision induced dissociation MS/MS technique.<sup>41</sup> However, in the case ESI-TOF MS analysis of  $[4 + O]^+$ , it was difficult to determine the accurate position of the Fe=O moiety (whether it is on iron porphycene or iron phthalocyanine in  $4^+$ ) even after MS/MS analysis of the  $[4 + O]^+$  peak because the ionization efficiency of the Fe-phthalocyanine fragments was much smaller than that of the Fe-porphycene fragments.

#### DFT Calculations.

Density functional theory (DFT) calculations were performed to gain further insight into experimental observations. The calculation details are presented in the Experimental section. We first focused on the electronic structure of  $4^+$  as well as its oxidized and reduced species. The electronic structure of  $4^+$  is very similar to that of  $[(\text{porphyrin})\text{Fe}_2\text{N}]^+$ , as described by Ghosh et al.<sup>42</sup> (Figure 7). The predicted Fe–N(Pc) and Fe–N(Ppc) average bond distance is 1.948 and 1.939 Å, respectively, which reasonably agrees with the experimental values of 1.94 and 1.93 Å, respectively (see Tables S1 and S2). The short Fe–N bond distances were consistent with the low-spin character of the Fe centers. The predicted Fe–N( $\mu$ ) bond lengths are 1.582 and 1.607 Å, respectively, which are systematically smaller than the X-ray data by approximately 0.05 Å.

Upon reduction, both Fe–N( $\mu$ ) bonds were lengthened as an antibonding orbital comprising Fe(3d<sub>z<sup>2</sup></sub>) and N(2s) orbitals. The difference between the two Fe–N( $\mu$ ) bonds is only 0.03 Å, indicating that the two Fe centers are similar and the complex could be formally characterized as Fe<sup>3.5</sup>–N–Fe<sup>3.5</sup>.<sup>20</sup> Spin populations also reveal that both Fe centers are involved in the reduction, with Fe(Pc) being slightly more reduced than Fe(Ppc). Upon oxidation, the Fe–N( $\mu$ ) bond lengths change by less than 0.01 Å, indicating that the oxidation occurs mainly at the macrocycles. The spin population of Pc is 0.76, whereas Ppc has a spin population of 0.15. This difference in the spin density implies that oxidation primarily occurs at Pc. The higher tendency of phthalocyanine to be oxidized is related to its longer conjugation length compared to that of porphycene.

We now compare the two oxo isomers, O=Fe(Pc)–N–Fe(Ppc) and O=Fe(Ppc)–N–Fe(Pc) (DFT structures are shown in Figure 7). Similar to a previous work,<sup>27</sup> two doublet states were calculated: the ground state in which one of the macrocycles was oxidized Fe<sup>IV</sup>Fe<sup>IV</sup>(P<sup>••</sup>) and a low-lying excited state Fe<sup>IV</sup>Fe<sup>V</sup> (Figure S4). Selected bond lengths are listed in Table S3. The Fe–N–Fe fragment is no longer symmetric. The general trend is that the formation of Fe-oxo significantly increases the length of the adjacent Fe–N( $\mu$ ) bond above 1.7 Å. DFT predicts that O=Fe(Pc)–N–Fe(Ppc) and O=Fe(Ppc)–N–Fe(Pc) are close in energy. The former isomer (in pyridine at 298 K) was slightly more stable (2–4 kcal mol<sup>-1</sup>) than the

latter (Table S5).

Considering that the phthalocyanine ring is more easily oxidized than the porphycene ring, H<sub>2</sub>O<sub>2</sub> might coordinate to Fe-porphycene more strongly than to Fe-phthalocyanine because the porphycene ring is more electron deficient than the phthalocyanine ring. This suggests that the oxo species of  $4^+$  could be preferentially generated on the Fe-porphycene moiety. This prompted us to compare the stability of the hydroperoxo species on the Fe-porphycene ring (HOOFePpc–N=FePc) with that of the Fe-phthalocyanine ring (HOOFePc–N=FePpc). We found that the difference between these two species is quite small (ca. 3 kcal mol<sup>-1</sup>; HOOFePpc–N=FePc is more stable than HOOFePc–N=FePpc). Moreover, we compared the O–O bond dissociation free energy in HOOFePpc–N=FePc and HOOFePc–N=FePpc because dissociation of the O–O bond is indispensable for the generation of iron-oxo species from hydroperoxo species. However, it was demonstrated that both hydroperoxo species have similar O–O bond dissociation free energy (37.2 kcal mol<sup>-1</sup> for HOOFePpc–N=FePc and 36.7 kcal mol<sup>-1</sup> for HOOFePc–N=FePpc in pyridine).

Considering the uncertainty in DFT calculations, the results obtained from DFT calculation propose that both oxo isomers (O=Fe(Pc)–N–Fe(Ppc) and O=Fe(Ppc)–N–Fe(Pc)) could be produced. However, it is also important to consider that the formation of oxo isomers should be kinetically controlled. The complete reaction mechanisms for the production of high-valent iron-oxo species are outside the scope of this study.

#### CH<sub>4</sub> Oxidation Activity.

We adopted the method developed by Sorokin et al. to evaluate the catalytic CH<sub>4</sub> oxidation activity of  $4^+ \cdot I_3^-$ .<sup>22</sup> H<sub>2</sub>O was used as the solvent for CH<sub>4</sub> oxidation because it is sufficiently stable against oxidation by high-valent iron-oxo species. For this purpose, we first prepared a silica gel-supported catalyst because  $4^+ \cdot I_3^-$  is not soluble in H<sub>2</sub>O. The CH<sub>4</sub> oxidation reaction was performed in an acidic aqueous solution containing 189 mM H<sub>2</sub>O<sub>2</sub> and 51 mM trifluoroacetic acid (TFA) at 60 °C under a CH<sub>4</sub> atmosphere of 1.0 MPa. After the oxidation reaction, MeOH, HCHO, and HCOOH were observed and quantified by GC-MS spectroscopy. The time dependence of each oxidized product is shown in Figure 8a and Table S7. The amount of oxidized products was significantly larger than that observed in the absence of CH<sub>4</sub>, suggesting that the observed MeOH, HCHO, and HCOOH were mostly derived from CH<sub>4</sub>. The small amount of oxidized products observed in the absence of CH<sub>4</sub> (under N<sub>2</sub> atmosphere) was mainly derived from the organic solvents adsorbed on the SiO<sub>2</sub> surface of the catalysts.<sup>21,28,31,32,43</sup>

To appropriately evaluate the catalytic CH<sub>4</sub> oxidation activity, the effective total turnover number (TTN<sub>eff</sub>) and effective methane

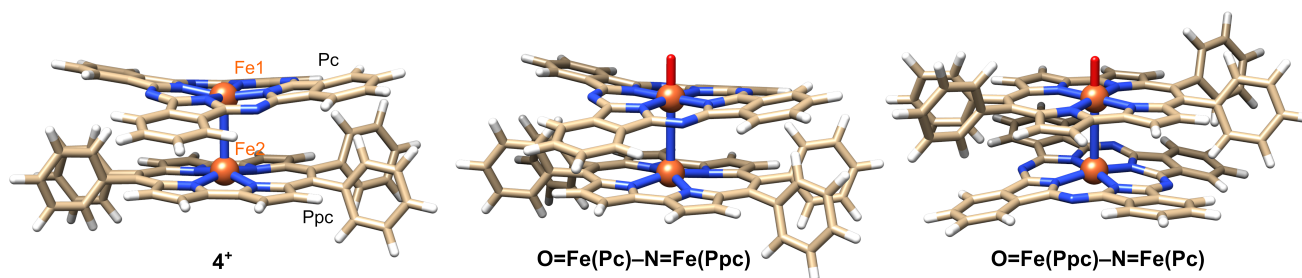


Figure 7 DFT structures of  $4^+$  and its isomeric oxo complexes.

conversion number ( $MCN_{\text{eff}}$ ) were defined according to equations (i)–(iv), based on the idea that  $\text{CH}_4$  is oxidized in a stepwise manner, as shown in Figure 8b.

$$TTN_{\text{eff}} = TTN_{(\text{CH}_4)} - TTN_{(\text{N}_2)} \quad (\text{i})$$

$$TTN_{(\text{CH}_4)} \text{ or } TTN_{(\text{N}_2)} = (C_{\text{MeOH}} + 2 \times C_{\text{HCHO}} + 3 \times C_{\text{HCOOH}}) / C_{\text{Catv}} \quad (\text{ii})$$

$$MCN_{\text{eff}} = MCN_{(\text{CH}_4)} - MCN_{(\text{N}_2)} \quad (\text{iii})$$

$$MCN_{(\text{CH}_4)} \text{ or } MCN_{(\text{N}_2)} = (C_{\text{MeOH}} + C_{\text{HCHO}} + C_{\text{HCOOH}}) / C_{\text{Catv}} \quad (\text{iv})$$

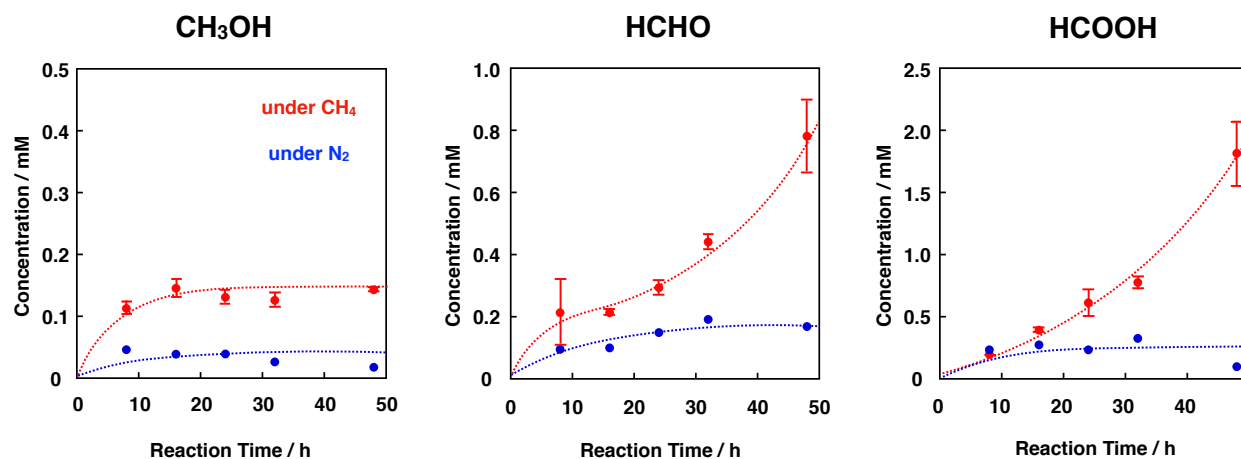
Figure 9a shows the time dependence of  $TTN_{\text{eff}}$ . Although  $TTN_{\text{eff}}$  increased almost linearly at the initial stage, the rate of increase increased, particularly after 32 h of oxidation. It should also be mentioned that the bluish-green color of the catalyst apparently became thinner, especially after 32 h, and almost colorless after 48 h of oxidation (Figure S5), suggesting that the porphyrinoid core of  $4^+\text{-I}_3^-$  gradually decomposed during the reaction. A similar bleaching of the color of the catalyst was observed in the oxidation reaction using the porphycene dimer  $3^+\text{-PF}_6^-$ . However, the bleaching speed was much slower for  $4^+\text{-I}_3^-$ , implying that the stability of  $4^+\text{-I}_3^-$  is higher than that of  $3^+\text{-PF}_6^-$  under these reaction conditions. Considering that apparent bleaching was not observed in the case of the phthalocyanine dimer  $1^+\text{-I}^-$ , the higher stability of  $4^+\text{-I}_3^-$  than  $3^+\text{-PF}_6^-$  might be because the phthalocyanine unit in  $4^+\text{-I}_3^-$  contributed to the stable generation of high-valent iron-oxo species after the reaction with  $\text{H}_2\text{O}_2$ .

To further investigate the reaction mechanism of  $\text{CH}_4$  oxidation by  $4^+\text{-I}_3^-$ , we performed  $\text{CH}_4$  oxidation in the presence of  $\text{Na}_2\text{SO}_3$ , a radical scavenger (Figure 9a and Table S7, entries 6 and 7).<sup>44</sup> It was demonstrated that the reaction after 24 h of oxidation was suppressed by approximately 63%, whereas the reaction after 48 h of oxidation was suppressed to 50%. This indicates that the oxidation reaction mainly proceeded through the high-valent iron-oxo species, at least in its initial stage. However, considering that

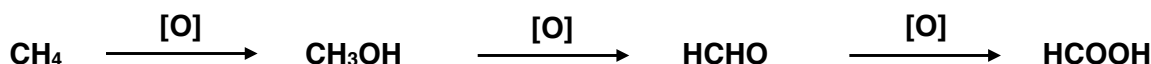
the color of  $4^+\text{-I}_3^-$  gradually bleached, particularly after 32 h, oxidation by the Fenton-type reaction via  $\bullet\text{OH}$  gradually increased, presumably because the decomposed product acted as the catalyst for the Fenton-type reaction, as summarized in Figure 9b. Because  $\bullet\text{OH}$  is so reactive that it can even decompose the porphyrinoid cores of  $4^+\text{-I}_3^-$ , the accelerated decomposition of the catalyst is not only because of the intrinsic instability of the catalyst, but also because of the decomposition by  $\bullet\text{OH}$ .

Figure 9c shows a comparison of  $TTN_{\text{eff}}$  and  $MCN_{\text{eff}}$  of  $1^+\text{-I}^-$ ,  $3^+\text{-PF}_6^-$ , and  $4^+\text{-I}_3^-$  after 24 h of oxidation under the same reaction conditions. The reason why  $4^+\text{-I}_3^-$  showed less  $\text{CH}_4$  oxidation activity than the porphycene dimer  $3^+\text{-PF}_6^-$  is that  $3^+\text{-PF}_6^-$  decomposed more rapidly and  $\text{CH}_4$  oxidation for 24 h mostly proceeded via a Fenton-type reaction. However, both  $TTN_{\text{eff}}$  and  $MCN_{\text{eff}}$  for oxidation by  $4^+\text{-I}_3^-$  were much less than in the case of oxidation by  $1^+\text{-I}^-$ , which mostly proceeded via high-valent iron-oxo species. Therefore, it can be concluded that the catalytic methane oxidation activity via the high-valent iron-oxo species of  $4^+\text{-I}_3^-$  ( $\text{O}=\text{FePpc}-\text{N}=\text{FePc}$  and/or  $\text{O}=\text{FePc}-\text{N}=\text{FePpc}$ ) is lower than that of the high-valent iron-oxo species of  $1^+\text{-I}^-$  ( $\text{O}=\text{FePc}-\text{N}=\text{FePc}$ ). This result indicates that the reactivity of the  $\mu$ -nitrido-bridged iron porphyrinoid dimer strongly reflects the difference in the porphyrinoid skeleton, although the structures of the  $\text{Fe}-\text{N}=\text{Fe}$  cores are quite similar. We consider that one possible explanation for the lower catalytic activity of  $4^+\text{-I}_3^-$  than  $1^+\text{-I}^-$  could be the slow generation of the high-valent iron-oxo species of  $4^+\text{-I}_3^-$  than that of  $1^+\text{-I}^-$  because of the lower efficiency of the push effect, which facilitates the heterolytic O–O bond cleavage of the hydroperoxo species ( $\text{Fe}-\text{O}-\text{OH}$ ) owing to the lower electron-donating ability of the porphyrinoid ring of  $4^+$ , as can be estimated from the fact that the oxidation potential of the phthalocyanine ring of  $4^+\text{-I}_3^-$  is higher than that of  $1^+\text{-I}^-$ .

(a)



(b)



**Figure 8** (a) Time dependence of the concentrations of each oxidized product (MeOH, HCHO, and HCOOH) observed in the reaction under  $\text{CH}_4$  atmosphere of 1.0 MPa (red filled circle) or in the absence of  $\text{CH}_4$  (under 1.0 MPa of  $\text{N}_2$ , blue filled circle) in an aqueous solution (3.0 mL) containing  $4^+\text{-I}_3^-/\text{SiO}_2$  (55  $\mu\text{M}$  as  $4^+\text{-I}_3^-$ ),  $\text{H}_2\text{O}_2$  (189 mM), and TFA (51 mM) at 60 °C. Error bars indicate standard deviations of three independent oxidation reactions. (b) Stepwise  $\text{CH}_4$  oxidation reaction.

## Conclusions

In this study, we synthesized a monocationic  $\mu$ -nitrido-bridged heterodimer of iron phthalocyanine and iron porphycene ( $4^+ \cdot I_3^-$ ) and investigated its electrochemical and spectroscopic properties. Single-crystal X-ray structural analysis demonstrated that the Fe–N=Fe core structure of  $4^+ \cdot I_3^-$  is similar to that of a monocationic  $\mu$ -nitrido-bridged iron phthalocyanine dimer ( $1^+ \cdot I^-$ ) and a monocationic  $\mu$ -nitrido-bridged iron porphycene dimer ( $3^+ \cdot PF_6^-$ ). ESI-TOF MS study indicated that treatment of  $4^+ \cdot I_3^-$  with  $H_2O_2$  gave the high-valent iron-oxo species of  $4^+$ . DFT calculations suggested that the high-valent iron-oxo species of  $4^+ \cdot I_3^-$  could be generated on both iron-porphycene and iron-phthalocyanine rings through the reaction with  $H_2O_2$ . The catalytic  $CH_4$  oxidation reaction by  $4^+ \cdot I_3^-$  in an acidic aqueous solution proceeded in the presence of excess  $H_2O_2$  to afford a mixture of MeOH, HCHO, and HCOOH through the high-valent iron-oxo species at its initial stage as in the case with  $1^+ \cdot I^-$ . It was demonstrated that the catalytic activity of the high-valent iron-oxo species of  $1^+ \cdot I^-$  was higher than that of  $4^+ \cdot I_3^-$ . However, as the reaction time was elongated, it was found that  $4^+ \cdot I_3^-$  was gradually decomposed. This implies that the high-valent iron-oxo species of  $4^+ \cdot I_3^-$  was less stable than that of  $1^+ \cdot I^-$ . Considering that the high-valent iron-oxo species of  $3^+ \cdot PF_6^-$  is much less stable and readily decomposes under the same reaction conditions, the lower stability of the high-valent iron-oxo species of  $4^+ \cdot I_3^-$  compared to that of  $1^+ \cdot I^-$  is derived from the difference in the porphyrinoid ring. Thus, it was confirmed that the difference in the porphyrinoid ring of the monocationic  $\mu$ -nitrido-bridged iron porphyrinoid dimer strongly affected the stability of the high-valent iron-oxo species as well as the catalytic activity of the monocationic  $\mu$ -nitrido-bridged iron porphyrinoid dimer. We believe that these findings would provide some valuable insights for the future development of molecular  $CH_4$  oxidation catalysts based on  $\mu$ -nitrido-bridged iron porphyrinoid dimers.

## Experimental

**General** All reagents and solvents were purchased at the highest commercial quality available and used without further purification, unless otherwise stated. A metal-free porphycene **3** was synthesized according to the reported procedure.<sup>45</sup>  $^1H$  NMR spectra were recorded on a JEOL JNM-ECS400 (400 MHz for  $^1H$ ) spectrometer at a constant temperature of 298 K. Elemental analysis was performed on a Yanaco MT-6 analyzer. The absorption spectrum was recorded with a Hitachi U-4100 spectrophotometer in pyridine solutions at  $20 \pm 0.1$  °C in 1.0 cm quartz cells. MALDI-TOF MS was performed on Bruker Daltonics ultrafleXtreme using  $\alpha$ -CHCA as a matrix. MALDI-TOF MS was performed on Bruker Daltonics compact.

**Synthesis of  $4^+ \cdot I_3^-$ .** A mixture of **5** (201 mg, 0.30 mmol), **6** (85 mg, 0.15 mmol),  $NaN_3$  (300 mg, 4.6 mmol) and 1-chloronaphthalene (7.5 mL) was heated under air at 280 °C for 2 hr. After cooling to room temperature, the reaction mixture was diluted with hexane (200 mL), the precipitate was collected by suction filtration, washed with hexane (400 mL)  $H_2O$  (300 mL), successively, dried under vacuum to give blackish green crude solid (392.3 mg). The crude product was dissolved in pyridine (400 mL). After iodine (70.2 mg, 0.55 mmol as I) was added, the resulting solution was stirred for 1h at room temperature, followed by evaporation of the volatile compounds. The residue was washed with  $Et_2O$  (300 mL) to remove the

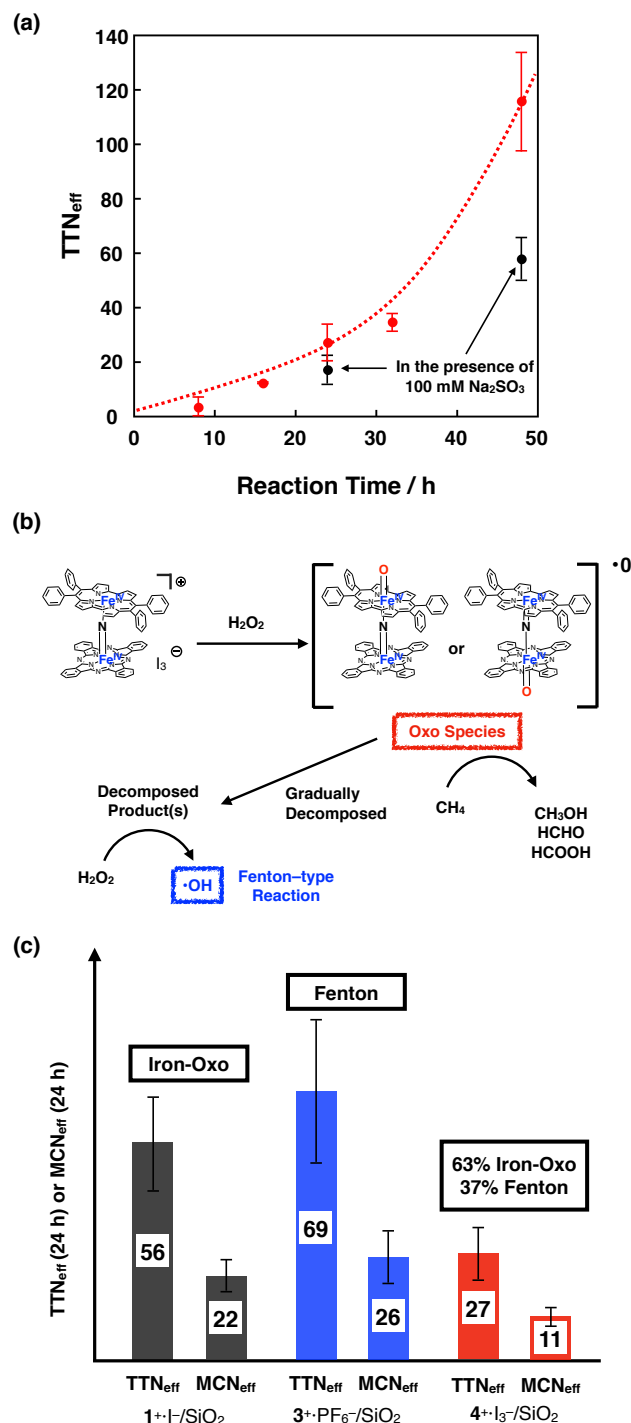


**Figure 9** (a) Time dependence of  $TTN_{eff}$  for  $CH_4$  oxidation by  $4^+ \cdot I_3^-$  in the absence (red circle) and presence (black circle) of 100 mM  $Na_2SO_3$ . Error bars indicate standard deviations of three independent oxidation reactions. (b) Proposed reaction mechanism for  $CH_4$  oxidation by  $4^+ \cdot I_3^-$ . (c) Comparison of  $TTN_{eff}$  and  $MCN_{eff}$  for  $CH_4$  oxidation for 24 h by  $1^+ \cdot I^-$ ,  $3^+ \cdot PF_6^-$ , and  $4^+ \cdot I_3^-$ .

remaining iodine, and then, dried under reduced pressure to give dark green solid. The crude was purified by silica gel column chromatography ( $4.5 \text{ cm} \phi \times 15.0 \text{ cm}$ ,  $CH_2Cl_2/ACOOEt = 10/10$ , then  $CH_2Cl_2/ACOOEt/MeOH = 10/10/1$ ) and recrystallization of  $CH_2Cl_2/Et_2O$  to yield  $4^+ \cdot I_3^-$  as a bluish green solid (121 mg, 89% (2 steps from a metal-free porphycene)).  $^1H$ -NMR (400 MHz, pyridine- $d_5$ /TMS):  $\delta =$

9.73 (dd,  $J = 5.4, 3.0$  Hz, 8H), 8.84 (d,  $J = 4.8$  Hz, 4H), 8.51 (dd,  $J = 6.0, 2.8$  Hz, 8H), 8.42 (d,  $J = 7.2$  Hz, 4H), 8.19 (d,  $J = 4.8$  Hz, 4H), 8.00 (t,  $J = 7.8$  Hz, 4H), 7.59 – 7.62 (m, 4H), 7.22 – 7.26 (m, 4H), 7.01 (d,  $J = 7.6$  Hz, 4H). MALDI-TOF MS :  $m/z = 1250.25$  : calcd for  $C_{76}H_{44}Fe_2N_{13}$  ( $[M]^+$ ) found: 1250.26. Anal. calcd for  $C_{164}H_{122}Fe_{46}N_{26}O_5$  ( $(4^+ \cdot I_3^-)_2 \cdot 3Et_2O \cdot 2H_2O$ ): C; 55.93, H; 3.49, N; 10.34, found: C; 55.66, H; 3.32, N; 10.04 (0.30% error).

**Synthesis of  $4^+ \cdot PF_6^-$ .**  $4^+ \cdot I_3^-$  (61 mg, 38  $\mu$ mol) was dissolved in 10 mL of acetonitrile. After  $KPF_6$  (691 mg, 3.8 mmol) in  $CH_3CN$  (10 mL) was added to the solution,  $H_2O$  (80 mL) was added. The resulting precipitate was collected by centrifugation, followed by decantation to yield dark green solid (54 mg). The crude product was further purified by PTLC ( $CH_2Cl_2/MeOH = 50/1$ ) and recrystallization from  $CH_2Cl_2/Et_2O$  to give the desired product  $4^+ \cdot PF_6^-$  as a bluish green solid (27.8 mg, 53%).  $^1H$ -NMR (400 MHz, pyridine- $d_5$ /TMS) :  $\delta = 9.72$  (dd,  $J = 5.6, 2.8$  Hz, 8H), 8.84 (d,  $J = 4.8$  Hz, 4H), 8.50 (dd,  $J = 5.6, 2.8$  Hz, 8H), 8.42 (d,  $J = 7.6$  Hz, 4H), 8.20 (d,  $J = 4.8$  Hz, 4H), 8.00 (t,  $J = 7.2$  Hz, 4H), 7.59 – 7.62 (m, 4H), 7.22 – 7.26 (m, 4H), 7.00 (d,  $J = 7.6$  Hz, 4H). MALDI-TOF MS :  $m/z = 1250.25$  : calcd for  $C_{76}H_{44}Fe_2N_{13}$  ( $[M]^+$ ) found: 1250.26. Anal. calcd for  $C_{76}H_{44}F_6Fe_2N_{13}P$  ( $4^+ \cdot PF_6^-$ ): C; 65.39, H; 3.18, N; 13.04, found: C; 65.45, H; 3.49, N; 13.14 (0.31% error).

**Single-Crystal X-ray Structural Analysis of  $4^+ \cdot I_3^-$ .** A  $4^+ \cdot I_3^-$  crystal suitable for single-crystal X-ray structural analysis was obtained by vapor diffusion of  $Et_2O$  into a  $4^+ \cdot I_3^-$  solution in a 1:1 (v/v) mixture of pyridine and  $CHCl_3$ . Single-crystal X-ray diffraction measurements were performed using a Rigaku X-ray diffractometer equipped with a molybdenum MicroMax-007 and Saturn 70 CCD detector. The measurement was performed at 123 K. The structure was solved via the direct method (SHELXT) and refined via full-matrix least-squares on  $F_2$  (SHELX-2018) using Olex2-1.3 program. All non-hydrogen atoms were refined anisotropically. Geometrical restraints were applied: DFIX, SADI, SIMU, ISOR, and OMIT. The crystal data are as follows: Formula  $C_{74}H_{49.6}Cl_{15.6}Fe_{1.6}I_{2.4}N_{12}$ , FW = 2053.882, crystal size  $0.19 \times 0.20 \times 0.22$  mm<sup>3</sup>, triclinic, space group  $P-1$ ,  $a = 20.6469(2)$  Å,  $b = 23.6627(3)$  Å,  $c = 24.8965(3)$  Å,  $\alpha = 64.380(1)^\circ$ ,  $\beta = 69.270(1)^\circ$ ,  $\gamma = 68.880(1)^\circ$ ,  $V = 9942.9(2)$  Å<sup>3</sup>,  $Z = 5$ ,  $R_1 = 0.1207$  ( $I > 2(I)$ ),  $wR_2 = 0.3227$  (all),  $GOF = 1.110$ . CCDC identification code 2217367. All the checkCIF Level-B alerts are due to the low crystal quality.

**Cyclic voltammogram of  $4^+ \cdot PF_6^-$ .** Cyclic voltammograms were measured with a BAS Electrochemical Analyzer Model 750Ds at room temperature in pyridine solutions containing 100 mM TBAPF<sub>6</sub> in a standard one-component cell under an  $N_2$  atmosphere equipped with a 3 mm-O.D. glassy carbon disk working electrode, platinum wire counter electrode, and Ag/AgCl reference electrode. All solutions were deoxygenated by  $N_2$  bubbling for at least 20 min. Obtained  $E^\circ$  vs. Ag/AgCl were converted to those vs.  $Fc/Fc^+$  based on measured redox potential of ferrocene. Tetrabutylammonium hexafluorophosphate ( $TBA^+PF_6^-$ ) was recrystallized from 95% EtOH and dried under vacuum overnight at 100 °C.

**ESI-TOF MS measurement of  $4^+ \cdot I_3^-$  in  $CH_3CN$  in the presence of  $H_2O_2$ .** To a solution of  $4^+ \cdot I_3^-$  in  $CH_3CN$  (1.0  $\mu$ M, 2.0 mL) was added 35% aqueous  $H_2O_2$  (0.1 mL, 1.16 mmol). After addition, the resulting mixture was subjected to ESI-TOF MS measurement immediately.

**DFT calculation.** DFT calculations were done with the BP86-D3(BJ)/def2-TZVP and B3LYP-D3(BJ)/def2-TVZP levels of theory implemented in the Turbomole software package.<sup>46</sup> The former functional was chosen based on the studies of Sorokin et al.<sup>20</sup> Only BP86 results were discussed, whereas the results calculated with B3LYP can be found in the Supporting Information. Frequency calculations were done to confirm the character of the optimized structures and to obtain Gibbs free energies. In some calculations, the solvent effect (pyridine) was determined using COSMO with a dielectric constant of 12.5.<sup>47</sup>

**Preparation of silica-supported catalyst ( $4^+ \cdot I_3^-/SiO_2$ ).**  $4^+ \cdot I_3^-$  (10.00 mg, 6.2  $\mu$ mol) was dissolved in 50 mL of mixture of pyridine and  $CHCl_3$  (1 : 1 (v/v)). After the addition of silica gel (1082 mg) to the solution, solvent was evaporated.  $CHCl_3$  (10 mL) was added to the residue. After solvent was evaporated, the residue was dried under vacuum at 60 °C over night. The catalyst was suspended in an aqueous TFA (TFA 10.0 mL +  $H_2O$  100 mL). The mixture was sonicated for 30 min and then the solid was filtered. This TFA wash procedure was repeated twice. Finally, the resulting solid was washed with  $H_2O$  (300 mL) and dried under vacuum at 60 °C over night. The silica-supported catalyst was obtained quantitatively.

**$CH_4$  oxidation reactions.** Heterogeneous  $CH_4$  oxidation was performed in a stainless-steel autoclave with a glass tube. A mixture containing the catalyst on  $SiO_2$  (30 mg, 55  $\mu$ M as  $4^+ \cdot I_3^-$ ), 35% aqueous  $H_2O_2$  (50  $\mu$ L, 189 mM), and TFA (12  $\mu$ L, 51 mM) in  $H_2O$  (3.0 mL) was heated at 60 °C under 1.0 MPa of  $CH_4$  for 8–48 h with continuous stirring (900 rpm). After the autoclave was opened, the reaction mixture was filtrated through a disposable membrane filter. The filtrate was analyzed by GC-MS (system: Agilent 7890A equipped with JEOL JMS-T100GCV, detection: EI, column: Agilent DB-WAX UI, external standard: isovaleric acid (5 mM), temperature conditions: initial: 70 °C to 220 °C (10 °C/min) – hold (5 min)). The yields of  $CH_3OH$  and formic acid were determined based on the results of GC-MS. The yield of formaldehyde was examined using the method reported in our previous paper.<sup>21,28,31,42</sup>

## Conflicts of interest

There are no conflicts to declare.

## Acknowledgements

This work was financially supported by a JSPS KAKENHI Grant-in-Aid for Scientific Research (A) (19H00902) and (B) (22H02094) awarded to KT, a JST PRESTO (Number 14J04135), a JSPS KAKENHI Grant-in-Aid for Challenging Exploratory Research (Number 22K19045), and a Grant-in-Aid for Scientific Research (B) (Number 19H02787 and 22H02156) awarded to YY. YY thanks to the financial supports by Tatematsu Foundation, Iwatani Naoji Foundation, and Toyoaki Scholarship Foundation.

## Notes and references

- 1 M. H. Sazinsky and S. J. Lippard, *Acc. Chem. Res.*, 2006, **39**, 558–566.



- 2 S. Sirajuddin and A. C. Rosenzweig, *Biochemistry*, 2015, **54**, 2283–2294.
- 3 V.C.-C. Wang, S. Maji, P. P.-Y. Chen, H. K. Lee, S. S.-F. Yu and S. I. Chan, *Chem. Rev.*, 2017, **117**, 8574–8621.
- 4 C. E. Tinberg and S. J. Lippard, *Acc. Chem. Res.*, 2011, **44**, 4, 280–288.
- 5 P. C. A. Bruijninx and B. M. Weckhuysen, *Angew. Chem. Int. Ed.*, 2013, **52**, 11980–11987.
- 6 Z. Guo, B. Liu, Q. Zhang, W. Deng, Y. Wang and Y. Yang, *Chem. Soc. Rev.*, 2014, **43**, 3480–3524.
- 7 S. J. Blanksby and G. B. Ellison, *Acc. Chem. Res.*, 2003, **36**, 255–263.
- 8 M. Ravi, M. Ranocchiari and J. A. van Bokhoven, *Angew. Chem. Int. Ed.*, 2017, **56**, 16464–16483.
- 9 F. T. de Oliveira, A. Chanda, D. Banerjee, X. Shan, S. Mondal, L. Que Jr., E. L. Bominaar, E. Münck and T. J. Collins, *Science*, 2007, **315**, 835–838.
- 10 G. Xue, R. D. Hont, E. Münck and L. Que Jr., *Nat. Chem.*, 2010, **2**, 400–405.
- 11 Y. Hitomi, K. Arakawa and M. Kodera, *Chem. Commun.*, 2014, **50**, 7485–7487.
- 12 E. Y. Tshuva and S. J. Lippard, *Chem. Rev.*, 2004, **104**, 987–1012.
- 13 X. Shan and L. Que Jr., *J. Inorg. Biochem.*, 2006, **100**, 421–433.
- 14 W. Nam, *Acc. Chem. Res.*, 2007, **40**, 522–531.
- 15 A. R. McDonald and L. Que Jr., *Coord. Chem. Rev.*, 2013, **257**, 414–428.
- 16 W. Nam, *Acc. Chem. Res.*, 2015, **48**, 2415–2423.
- 17 M. Guo, T. Corona, K. Ray and W. Nam, *ACS Cent. Sci.*, 2019, **5**, 13–28.
- 18 J. E. M. N. Klein and G. Knizia, *Angew. Chem. Int. Ed.*, 2018, **57**, 11913–11917.
- 19 D. R. Weinberg, C. J. Gagliardi, J. F. Hull, C. F. Murphy, C. A. Kent, B. C. Westlake, A. Paul, D. H. Ess, D. G. McCafferty and T. J. Meyer, *Chem. Rev.*, 2012, **112**, 4016–4093.
- 20 P. Afanasiev and A. B. Sorokin, *Acc. Chem. Res.*, 2016, **49**, 583–593.
- 21 Y. Yamada, J. Kura, Y. Toyoda and K. Tanaka, *Dalton Trans.*, 2021, **50**, 6718–6724.
- 22 A. B. Sorokin, E. V. Kudrik and D. Bouchu, *Chem. Commun.*, 2008, 2562–2564.
- 23 E. V. Kudrik, P. Afanasiev, L. X. Alvarez, P. Dubourdeaux, M. Clémancey, J.-M. Latour, G. Blondin, D. Bouchu, F. Albrieux, S. E. Nefedov and A. B. Sorokin, *Nat. Chem.*, 2012, **4**, 1024–1029.
- 24 C. Colombari, E. V. Kudrik, V. Briois, J. C. Shwarbrick, A. B. Sorokin and P. Afanasiev, *Inorg. Chem.*, 2014, **53**, 11517–11530.
- 25 M. G. Quesne, D. Senthilnathan, D. Singh, D. Kumar, P. Maldivi, A. B. Sorokin, S. P. de Visser, *ACS Catal.*, 2016, **6**, 2230–2243.
- 26 M. Ansari, N. Vyas, A. Ansari, G. Rajaraman, *Dalton Trans.*, 2015, **44**, 15232–15243.
- 27 Q. M. Phung and K. Pierloot, *Chem. Eur. J.*, 2019, **25**, 12491–12496.
- 28 Y. Yamada, Y. Miwa, Y. Toyoda, T. Yamaguchi, S. Akine and K. Tanaka, *Dalton Trans.*, 2021, **50**, 16775–16781.
- 29 G. Anguera, D. Sánchez-García, *Chem. Rev.*, 2017, **117**, 2481–2516.
- 30 J. Waluk, *Chem. Rev.*, 2017, **117**, 2447–2480.
- 31 Y. Yamada, K. Morita, N. Mihara, K. Igawa, K. Tomooka and K. Tanaka, *New J. Chem.*, 2019, **43**, 11477–11482.
- 32 N. Mihara, Y. Yamada, H. Takaya, Y. Kitagawa, K. Igawa, K. Tomooka, H. Fujii and K. Tanaka, *Chem. Eur. J.*, 2019, **25**, 3369–3375.
- 33 Ü. İ. Ş. Çi, A. S. Faponle, P. Afanasiev, F. Albrieux, V. Briois, V. Ahsen, F. Dumoulin, A. B. Sorokin, S. P. de Visser, *Chem. Sci.*, 2015, **6**, 5063–5075.
- 34 K. M. Kadish, R. K. Rhodes, L. A. Bottomley and H. M. Goff, *Inorg. Chem.*, 1981, **20**, 3195–3200.
- 35 L. A. Bottomley and B. B. Garrett, *Inorg. Chem.*, 1982, **21**, 1260–1263.
- 36 M. Li, M. Shang, N. Ehlinger, C. E. Schulz and W. R. Scheidt, *Inorg. Chem.*, 2000, **39**, 580–583.
- 37 Y. Yamada, T. Sugiura, K. Morita, H. Ariga-Miwa and K. Tanaka, *Inorg. Chim. Acta*, 2019, **489**, 160–163.
- 38 T. Shimizu, K. Wakamatsu, Y. Yamada, Y. Toyoda, S. Akine, K. Yoza and H. Yoshikawa, *ACS Appl. Mater. Interfaces*, 2021, **13**, 40612–40617.
- 39 L. A. Bottomley, J.-N. Gorce, V. L. Goedken and C. Ercolani, *Inorg. Chem.*, 1985, **24**, 3733–3737.
- 40 C. Bernard, J. P. Gisselbrecht, M. Gross, E. Vogel and M. Lausmann, *Inorg. Chem.*, 1994, **33**, 2393–2401.
- 41 C. Colombari, E. V. Kudrik, A. B. Sorokin, *J. Porphyrins Phthalocyanine*, 2017, **21**, 346–353.
- 42 A. Ghosh, E. Tangen, E. Gonzalez and L. Que, *Angew. Chem.*, 2004, **116**, 852–856.
- 43 Y. Yamada, J. Kura, Y. Toyoda and K. Tanaka, *New J. Chem.*, 2020, **44**, 19179–19183.
- 44 C. Hammond, M. M. Forde, M. H. Ab Rahim, A. Thetford, Q. He, R. L. Jenkins, N. Dimitratos, J. A. Lopez-Sanchez, N. F. Dummer, D. M. Murphy, A. F. Carley, S. H. Taylor, D. J. Willock, E. E. Stangland, J. Kang, H. Hagen, C. J. Kiely and G. J. Hutchings, *Angew. Chem. Int. Ed.*, 2012, **51**, 5129–5133.
- 45 T. Ono, N. Xu, D. Koga, T. Ideo, M. Sugimoto, Y. Hisaeda, *RSC Adv.*, 2018, **8**, 39269–39273.
- 46 S. G. Balasubramani, G. P. Chen, S. Coriani, M. Diedenhofen, M. S. Frank, Y. J. Franzke, F. Furche, R. Grotjahn, M. E. Harding, C. Hättig, A. Hellweg, B. Helmich-Paris, C. Holzer, U. Huniar, M. Kaupp, A. Marefat Khah, S. Karbalaee Khani, T. Müller, F. Mack, B. D. Nguyen, S. M. Parker, E. Perlt, D. Rappoport, K. Reiter, S. Roy, M. Rückert, G. Schmitz, M. Sierka, E. Tapavicza, D. P. Tew, C. van Wüllen, V. K. Voora, F. Weigend, A. Wodyński and J. M. Yu, *J. Chem. Phys.* 2020, **152**, 184107.
- 47 A. Klamt and G. Schüürmann, *J. Chem. Soc. Perkin Trans. 2*, 1993, 799–805.